ADVANCED MATERIALS
www.advmat.de

Terahertz Electronic and Spin Currents in Wafer-Scale Van der Waals Bi_2Se_3/WSe_2 Heterostructures and Polymorphs

M. Mičica, A. Wright, S. Massabeau, S. Ayari, E. Rongione, M. Oliveira Ribeiro, S. Husain, R. Sharma, T. Denneulin, R. E. Dunin-Borkowski, J. Mangeney, J. Tignon, R. Lebrun, H. Okuno, O. Boulle, A. Marty, F. Bonell, F. Carosella, H. Jaffrés, R. Ferreira, J.-M. George, M. Jamet, and S. Dhillon**

Van der Waals heterostructures and polymorphs have promised the realization of artificial materials with multiple physical phenomena such as giant optical nonlinearities, spin-to-charge interconversion in spintronics and topological carrier protection, through an infinitely diverse set of 2D quantum materials and their stacking order in a single layered device. However, their exploitation for the terahertz range has been limited with most investigations based around the optical domain, owing to the use of exfoliated material that inherently limits both the dimensions of the materials and the scalability for applications. Here, the combination of terahertz electronic and spin currents is demonstrated through the realization of large area complex crystalline heterostructures of topological insulators, transition metal dichalcogenides (TMDs) and ferromagnets. This is demonstrated through down-conversion of optical beams into coherent terahertz currents, where the terahertz phase permits the decoupling of the physical phenomena, and bringing novel functionalities beyond those achievable in simple homostructures. In particular, the role of different TMD polymorphs (stacking orders - 1T′, 2H, and 3R) is shown with the simple change of one atomic monolayer of the material stack entirely changing the terahertz responses – both electrical and magnetic - of the artificial material. This allows to highlight ultrafast phenomena that combine both the electronic- and spin-based processes in these structures. The importance of the crystal symmetry on the magnetic properties through proximity effects is further demonstrated, showing a nonlinearity of magnetic origin as a result of the 1T′ polymorph. As well as control of the terahertz currents through different polymorphs, this scalable integration of a set of highly diverse materials establishes a platform for next-generation 2D heterostructures that integrate photonic, electronic, and spintronic properties into device architectures.

1. Introduction

The potential of van der Waals (vdW) heterostructures[1–5] is vast with the possibilities of combining a myriad of physical phenomena such as superconductivity, valleytronics, giant optical nonlinearities, proximity effects and spintronics, in a single artifically created material. It can be achieved through the design and realization of quantum interfaces and structures by combining materials as diverse as graphene, 2D transition metal dichalogenides (TMD) and their polymorphs, topological insulators (TIs), 2D ferromagnets, 2D ferroelectrics and many more. This has led to the term of atomic-scale Lego that is facilitated by the absence of dangling bonds in vdW materials. Nevertheless, the vast majority of works that have been performed are based on exfoliation from bulk crystals and manual stacking of individual layers. This inherently inhibits scalability and applications of complex vdW heterostructures. However, recent developments in epitaxial growth of TMDs have shown that large area 2D crystalline materials are starting to become available,[6–8] opening up new possibilities of complex heterostructures. In this work, we show wafer scale epitaxially grown heterostructures of TIs,[9] 2D TMD[10] polymorphs and ultrathin

The ORCID identification number(s) for the author(s) of this article can be found under https://doi.org/10.1002/adma.202506031

DOI: 10.1002/adma.202506031

M. Mičica, A. Wright, S. Ayari, E. Rongione, J. Mangeney, J. Tignon, F. Carosella, R. Ferreira, S. Dhillon
Laboratoire de Physique de l'Ecole Normale Supérieure, ENS
Université PSL, CNRS
Sorbonne Université
Université Paris Cité
Paris F-75005, France
E-mail: sukhdeep.dhillon@phys.ens.fr

ferromagnets. This opens up exciting prospects of combining multiple effects in the same 2D stack. Here we demonstrate the control of the material's ultrafast transport and terahertz (THz) properties through polymorph dependent optical nonlinearities, ultrafast spin-to-charge conversion (SCC), magnetic proximity effects and anisotropic charge properties over macroscopic surface areas with sensitivity to the monolayer limit.

Regarding the state-of-the-art, over the last decade, layered 2D materials such as TIs,[9] Rashba materials[11] and TMDs[10] and their corresponding quantum interfaces have taken a central role in the range of condensed matter phenomena including, but not limited to:

i) Spin-to-charge interconversion (SCC) where the harvesting of strong spin-orbit coupling (SOC) in quantum interfaces has been applied to a diverse range of applications. In particular, SCC in TI interfaces have demonstrated a rich physics playground owing to their exotic bandstructure properties,[12,13] where their electronic band dispersion is composed of a 'bulk' insulating form and Dirac-like topologically-protected conducting surface states within the gap. Recent studies have also investigated ultrafast SCC through THz emission studies where TI/ferromagnet junctions are optically excited to generate a spin current in the ferromagnet and converted into a charge current in the TI.[14–19] Similarly, TMDs with large spin-orbit coupling have been studied, with the layer-by-layer control permitting to engineer and control the SCC processes.[20]

ii) Magnetic proximity effects that have recently emerged, which provide a unique method of engineering 2D materials.[21] Here the inherent compatibility of 2D materials permits a strong interfacial interaction between two entirely different 2D materials i.e non-magnetic and magnetic, modifying each of the layer properties. This permits, for example, to induce magnetic phenomena in the non-magnetic material and has shown, for example, proximity-induced magnetism at the interface between a topological insulator and a ferromagnet, probed using magnetic nonlinearities.[22] This has allowed prospects in the control of magnetic ordering, spintronics and valleytronics without the need of magnetic doping or the use of defects that can negatively impact the crystal structure of 2D materials.

iii) Giant optical nonlinearities, where a wide range of work has been applied to second harmonic generation (SHG) in 2D TMDs, such as WSe_2,[23,24] MoS_2,[25] $MoSe_2$,[26] and more.[27,28] These materials have shown considerable advances with their electronic, optical and nonlinear properties controllable by the number of layers, as well as the layer polymorph of the material.[29] Indeed, the layer polymorph, corresponding to the stacking order of the 2Ds layer has shown to be an important parameter in the control of SHG. This has been demonstrated in, for example, the 2H or 3R stacking in typical TMDs or in ReS_2 with distinct differences between 1T′ and non-centrosymmetric 2H-polymorphs.[30] Note that in SHG experiments usually only the intensity is measured (accessing phase information requires more complex heterodyne detection methods,[31,32]) while the THz emission experiments are inherently resolved in amplitude and phase.

However, the majority of these studies, especially those with TMDs, have been limited to small individual crystals or exfoliated materials, constrained to one single phenomena, and limiting the reproducibility at scale despite considerable progress in centimetre scale exfoliated materials.[33,34] This has also restricted the study of these materials mostly to the visible/infrared regions of the electromagnetic spectrum. Exfoliated material and relatively large areas can be used for THz experiments, such as recent demonstrations of THz nonlinearities in thick vdW layers (for example in $NbOI_2$[35]) but have not been extensively applied to complex heterostructures with multiple heterostructure control. Such effects on large surface areas have been limited owing to the requirement of high quality epitaxial growth of monolayers (MLs). Recent work, however, has shown that the field is progressing rapidly, with demonstrations of polymorph control,[36] ultrafast photocurrents[37–39] and carrier dynamics,[40,41] mid-infrared detection,[42] layered controlled THz spintronic emission[20] and mid-infrared harmonic generation.[43,44]

In this work, we show the combination of 2D giant optical nonlinearities, THz spintronics and magnetic proximity-induced effects in epitaxal large area TI/TMD/FM heterostructures. After demonstrating the epitaxial growth of TI/TMD/FM (Bi_2Se_3/WSe_2/Co) with a varying thickness of the WSe_2 layers at the atomic level, we report on combined physical phenomena in the 2D stack: *i*) ultrafast spin-to-charge conversion from optically excited spin current in the FM to the TI and the TMD; *ii*) THz nonlinear current generation through optical nonlinearities from the TI and TMD; and *iii*) how the TMD polymorph can be used to control the nonlinearities, the anisotropic response, and the proximity-induced magnetic properties at the ML level. Previous work on TI/TMD grown heterostructures is limited and has been focused primarily on the growth of large area domains.[45] No investigations have shown on their electronic and photonic properties that can be controlled layer-by-layer, the nature of the polymorphs or the use of mis-cut substrates for grain alignment. Further no magnetic-based phenomena have been demonstrated.

Figure 1a shows the schematic of our approach. Here, a femtosecond near infrared laser, E_{NIR}, is used to excite a 2D heterostructure of the FM, TMD and TI quantum layers at normal incidence. The FM permits the generation of an ultrafast spin polarised current (j_s) that is converted into a charge current (j_c) at the surface of TI, whilst both the TMD and TI possess photoexcited nonlinear currents owing to their second order nonlinearities $\chi^{(2)}$. Both these effects result in a radiating electromagnetic pulse through the down-conversion of the optical beam to the THz region E_{THz}. Figure 1b,c shows schematically the effect of

S. Massabeau, E. Rongione, S. Husain, R. Lebrun, H. Jaffrés, J.-M. George
Laboratoire Albert Fert, CNRS, Thales
Université Paris-Saclay
Palaiseau 91767, France

S. Ayari
De Vinci Higher Education
De Vinci Research Center
Paris, France

M. O. Ribeiro, R. Sharma, O. Boulle, A. Marty, F. Bonell, M. Jamet
Univ. Grenoble Alpes, CEA, CNRS
Grenoble INP, IRIG-SPINTEC
Grenoble F-38000, France
E-mail: matthieu.jamet@cea.fr

T. Denneulin, R. E. Dunin-Borkowski
Ernst Ruska-Centre for Microscopy and Spectroscopy with Electrons
Forschungszentrum Jülich
D-52425 Jülich, Germany

H. Okuno
Univ. Grenoble Alpes, CEA, IRIG-MEM
Grenoble 38000, France

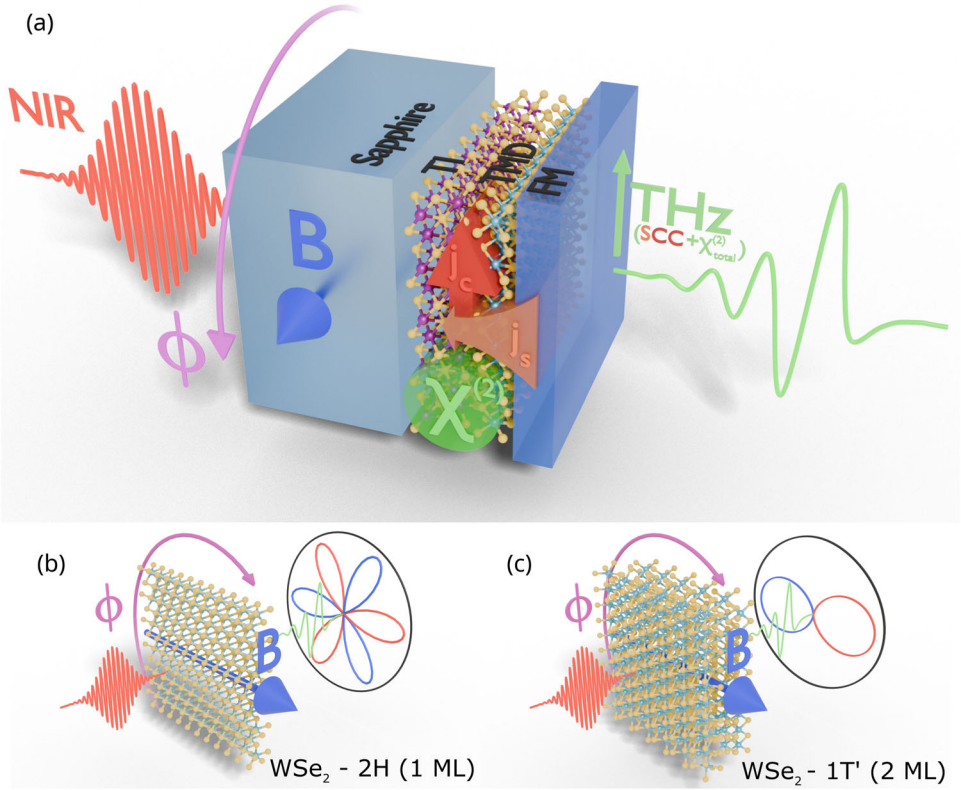

Figure 1. Schematic of TI/TMD/FM heterostructure a) A femtosecond laser pulse excites the whole structure and generates THz radiation by i) SCC at the TI interface and in the TMD, owing to the flow of spin current j_s from FM and the generation of j_c and ii) by the second order nonlinearities $\chi^{(2)}_{total}$ (see Equation (3)) possessed by both the surface states of the TI and the TMD. The TMD also possesses a magnetic dependent nonlinearity $\chi^{(2)}_c$ induced by its proximity with the FM (see Equation 3). The heterostructure is on a sapphire substrate that is rotated around its azimuthal angle ϕ independently of the fixed external magnetic field B. (b-c) Shows an illustration of azimuthal dependence of emitted THz pulse with the different physical contributions, nonlinear (red/blue) and magnetic (black) origin, for different polytypes of WSe_2, 2H and 1T′ with 1 ML and 2 ML, respectively.

isotropic (1 ML) and anisotropic (2 ML) WSe_2 response, respectively, with the expected azimuthal dependence of the generated THz field from the nonlinearity, where the symmetry of the WSe_2 plays a crucial role (red/blue curves, see below), and the spin-to-charge conversion (black curve). The WSe_2 layer, as well as preserving the surface states of the TI,[15,17,46,47] also acts as a tunnel barrier in analogy of spin injection studies on metallic spintronic layers.[48]

A key point of this work is on the crystal structure of the TMD structure over large surface areas and its role in the nonlinear and magnetic properties of the heterostructure. Indeed, TMDs are known to have different polymorphs that can effect their optical, electronic and multiferroic responses.[49–52] **Table 1** shows the typical polymorphs observed in the TMD WSe_2 and the expected nonlinear and magnetic response with azimuthal angle. The structural representation of 1T′, 2H and 3R TMD polytypes together with their atom coordination are shown. (The numbers indicate the number of layers in the unit cell and the letters stand for trigonal, hexagonal and rhombohedral, respectively. 1T′ is a result of the structure distortion of the 1T polymorph). For the 3R polymorph, the structure is non-centrosymmetric and a second order intrinsic nonlinearity $\chi^{(2)}_i$ is expected no matter the number of layers.[53] For the 2H (1T′) polymorph, the $\chi^{(2)}_i$ is only present for odd (even) number of layers owing to even (odd) layers being centrosymmetric.[53] The form of the second order polarization as a function of azimuthal angle, ϕ is shown in the 5th row. In the case of 3R and 2H, in the presence of a $\chi^{(2)}_i$, the expected form corresponds to a sixfold rotation symmetry, owing to the three-fold symmetry of a typical TMD (reduced point group D_{3h} for 2H and C_{3v}):

$$\chi^{(2)}_i = d_{26}\cos 3\phi \tag{1}$$

where d corresponds to the non-zero nonlinear tensor for this polymorph. However, for the case of 1T′, in the presence of a $\chi^{(2)}_i$ (even layers), the expected symmetry changes drastically to 2-fold owing to the reduced symmetry of the space group C^1_s.[54]

$$\chi^{(2)}_i = d_{11}\cos^3\phi + (d_{12}+2d_{26})\cos\phi\sin^2\phi \tag{2}$$

The details of the calculated nonlinear susceptibility using DFT simulations is given in the Supporting Information The magnetic response (THz emission of spin origin, 6th row) with azimuthal angle is expected to be isotropic at the TMD or TI surface for each of the polymorphs, as the origin is from spin-to-charge conversion (through the Inverse Spin-Hall or Edelstein Effects).

Table 1. Comparison of different polytypes 2H, 3R and 1T′ of WSe_2. The first and second row show the struture of the layers (top and side views), the third and fourth show the behavior of second order nonlinearity χ^2 for different number of layers, the fifth row shows the calculated azimuthal dependence of the real part of the nonlinearity (red = positive, blue = negative values). The sixth row shows the expected magnetic response of the stack with the azimuthal dependence of the SCC (black) and magnetic dependent nonlinearity (red/blue curve).

Polytype	2H	3R	1T′
Top view	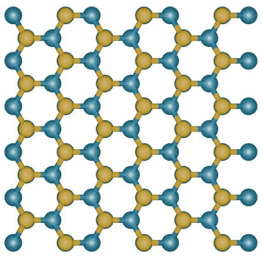	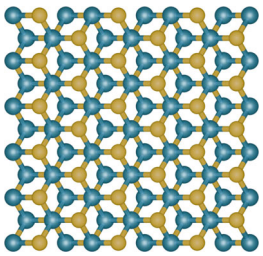	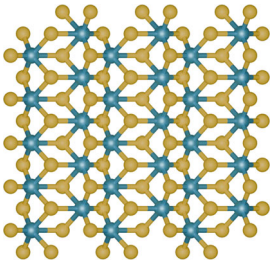
Side view	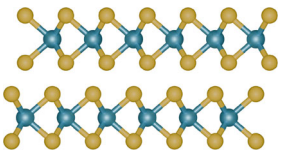	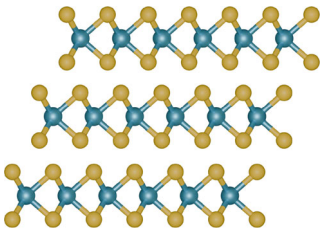	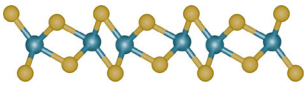
Odd # ML	$\chi^2 \neq 0$	$\chi^2 \neq 0$	$\chi^2 = 0$
Even # ML	$\chi^2 = 0$	$\chi^2 \neq 0$	$\chi^2 \neq 0$
Nonlinear(ϕ)	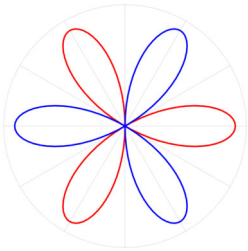	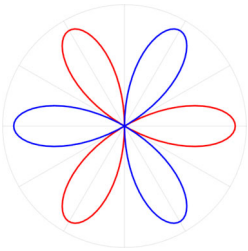	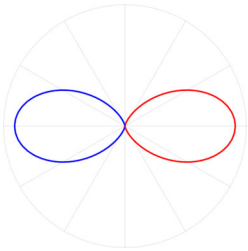
Magnetic(ϕ) (TI/TMD /FM)	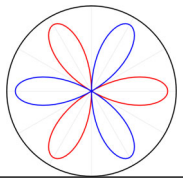	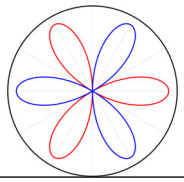	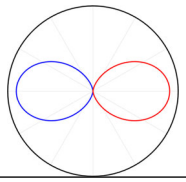

However, owing to proximity effects between the ferromagnetic and the TMD layer a small magnetic field nonlinearity is induced with a similar azimuthal response to the nonlinear $\chi_i^{(2)}$ response, as shown in Table 1, but with a non-trivial response with number of atomic layers. Indeed the total nonlinearity $\chi_{total}^{(2)}$ is given by:

$$\chi_{total}^{(2)} = \chi_i^{(2)} \pm \chi_c^{(2)} \tag{3}$$

where $\chi_c^{(2)}$ is the magnetic nonlinearity, referred to as c-type that reverses sign when the magnetic field is reversed. Typically i-type is orders of magnitude larger than c-type, and therefore the magnetic nonlinearity is often neglected. However, recent work has shown that the c-type nonlinearity can have a important contribution to the total nonlinearity in 2D materials,[55,56]

Note that in such semiconducting TMDs the electronic band structure changes with the layer thickness, with a direct bandgap for ML TMDs to an indirect bandgap for greater number of MLs.[57] For WSe_2 2H and 3R stacked bilayers, the bandgap energy is ≃1.8 eV and 1.3 eV ≃ for bulk,[58,59] respectively. For the 1T′ polymorph, reports have shown small bandgap energies of around 100 meV[60,61] for 1 ML or semi-metal behavior. The bandstructures of each polymorph are presented in the Supporting Information

2. Growth and Structural Characterization of Epitaxial TI/TMD/FM Heterostructures

All the Bi_2Se_3(10QL)/WSe_2(t_{TMD}) heterostructures were grown by molecular beam epitaxy (MBE) on large area c-cut sapphire

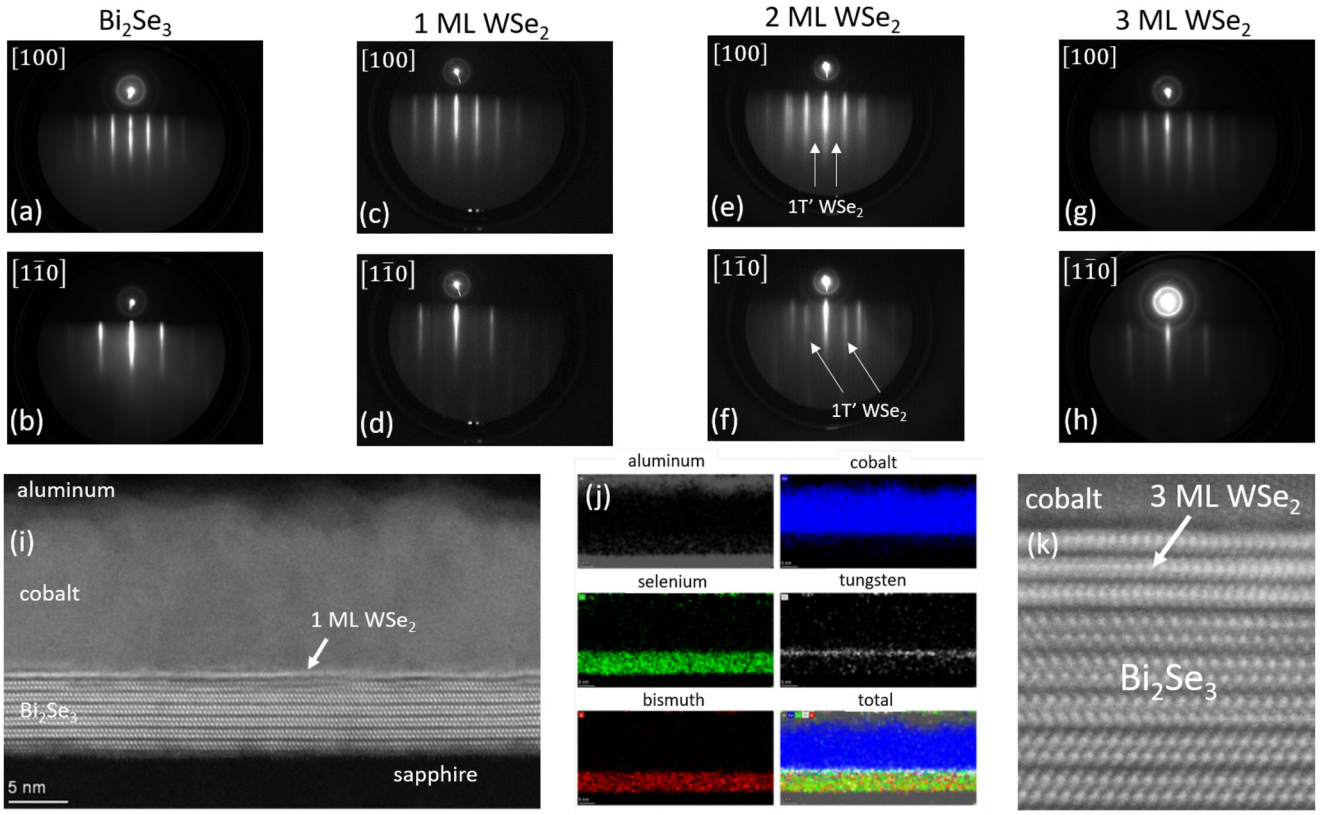

Figure 2. Structure and polymorph characterisation of TI/TMD/FM heterostructure. a–h) RHEED patterns recorded along two azimuths [100] and [1$\bar{1}$0] of 10 QL of Bi_2Se_3 and 1-3 ML of WSe_2. i) STEM cross-section image of Bi_2Se_3(7QL)/WSe_2(1ML)/Co(10nm)/Al(3nm). (This stack had a thinner Bi_2Se_3 and a thicker Co layer than that tested for the THz measurements). j) Corresponding elemental chemical analysis by EDX of the Bi_2Se_3(7QL)/WSe_2(1ML)/Co(10nm)/Al(3nm) stack: aluminum (dark grey), cobalt (blue), selenium (green), tungsten (white) and bismuth (red). k) Atomic scale STEM cross section image of Bi_2Se_3(10QL)/WSe_2(3ML)/Co(3nm)/Al(3nm) showing the vdW gaps, Co/WSe_2 and WSe_2/Bi_2Se_3 interfaces.

substrates, with the details provided in the Methods section (QL - quintuple layers). These substrate types have shown the possibility of oriented TMD epitaxial growth for wafer scale single crystal films owing to their miscut nature.[62] t_{TMD} corresponds to the WSe_2 layer thickness (1, 2, 3, and 4 MLs). A low growth temperature was chosen to favor the presence of multi-polymorphs of WSe_2. 3 nm of cobalt (Co) and aluminum (Al) were then evaporated by e-beam at room temperature at 0.1 and 0.5 Ås^{-1} rates, respectively. The aluminium oxidises to provide a AlO_x protective insulating layer of the heterostructure.

The reflection high energy electron diffraction (RHEED) patterns are shown in **Figure** 2a–h. The two distinct patterns along [100] and [1$\bar{1}$0] azimuths demonstrate the single crystalline character of the layers. We also clearly see the epitaxial relationship between the successive layers and the presence of thin streaks indicates the atomically flat character of the films as expected for the layer-by-layer growth of 2D materials. Co and Al are polycrystalline with RHEED patterns exhibiting rings. Regarding the different possible polymorphs of WSe_2, in the RHEED patterns recorded along the [100] direction, we observe faint lines in-between the first order diffraction lines resembling a (x2) surface reconstruction. This diffraction pattern is characteristic of the presence of the 1T′ polymorph of WSe_2 at the surface of the film.[60,63,64] The low growth temperature promotes the formation of this polymorph and is also necessary to avoid damaging the Bi_2Se_3 layer that starts decomposing above 300°C. The presence of the 1T′ polymorph is more visible for 2 ML of WSe_2 as highlighted in Figure 2e,f. Scanning transmission electron microscopy (STEM) images in cross section are shown in Figure 2i,k for 1 ML and 3 ML of WSe_2, respectively. We can clearly observe van der Waals gaps between the Bi_2Se_3 QLs and WSe_2 MLs. Moreover, as shown in Figure 2k, Co/WSe_2 and WSe_2/Bi_2Se_3 interfaces are atomically sharp and appear as quasi-vdW gaps in the STEM image. Regarding other stacking orders, the 2H polymorph is observed for 2 MLs and a mixture of 3R and 2H polymorphs for layers greater than 2 MLs. The details about the stacking of WSe_2 layers are given in the Supporting Information In Figure 2j, the elemental chemical analysis by energy dispersive x-ray spectroscopy (EDX) corresponding to the STEM image of Figure 2i confirms the absence of atomic intermixing at the Co/WSe_2 interface and the role played by WSe_2 as a diffusion barrier between the ferromagnet and the TI avoiding selenium diffusion into the cobalt layer.

To summarise, 1T′ is present in all samples, 2 MLs has a 2H polymorph and thicker layers shows a mixture of 3R and 2H polymorphs. Raman spectroscopy was also performed to verify the monolayer nature and thickness of the deposited WSe_2 spacer (see Supporting Information). The evolution of the Raman shifts are in close agreement with the literature on WSe_2 layers.[65] The

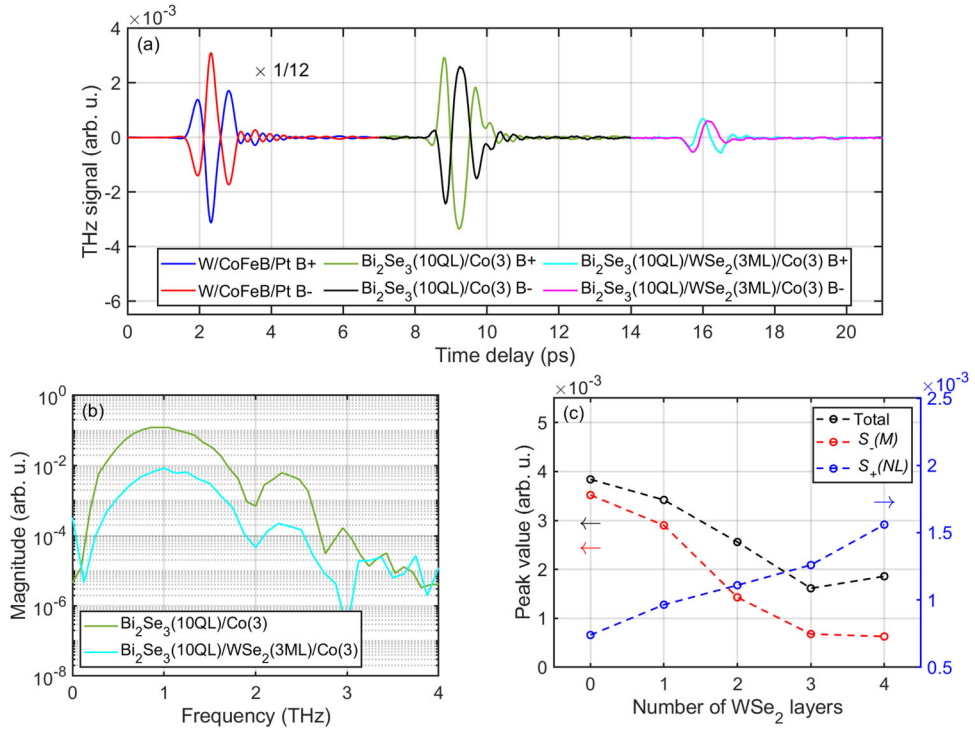

Figure 3. Evolution of THz amplitude for nonlinear and spintronic processes with WSe_2 barrier thickness. a) THz emission from Bi_2Se_3/Co/AlO_x and Bi_2Se_3/WSe_2(3ML)/Co/AlO_x compared to W/CoFeB/Pt at two opposite magnetic field polarities B±. The curves for each sample are shifted in time for clarity. b) THz spectrum from the Bi_2Se_3/Co/AlO_x and Bi_2Se_3/WSe_2(3ML)/Co/AlO_x samples showing a bandwidth of approximately 3 THz (detection limited). c) Evolution of the total (black), $S_-(M)$ (red) and $S_+(NL)$ (blue curve) contributions from Bi_2Se_3/WSe_2(t_{TMD})/Co/AlO_x as a function of the WSe_2 number of layers, t_{TMD}, ranging from 0 to 4 ML. All stacks had 10 QLs of Bi_2Se_3, 3 nm of Co and 3 nm of AlO_x.

Supporting Information also shows the large area uniformity on microscopic and macroscopic surface areas of the realised samples.

3. Coherent Current Transport via THz Emission Spectroscopy

We now move to down-conversion in these Bi_2Se_3/WSe_2/Co heterostructures through coherent THz emission spectroscopy where an ultrafast optical excitation is downconverted to the THz range via ultrafast currents through two particular phenomena:

i) Optical nonlinear conversion where a resonant or non-resonant optical excitation results in second order nonlinearities for ultrafast current generation through optical rectification for THz generation, similar to SHG:

$$E_{\mathrm{THz}} \propto \chi^{(2)}_{total}(\phi) E_{NIR} E^{*}_{NIR} \tag{4}$$

where E_{THz} is the emitted THz field and E_{NIR} corresponds to the electric field of the optical excitation, and

ii) Spintronic THz emission that relies on the ultrafast demagnetization of the thin ferromagnetic layer and transient SCC in a strong spin-orbit coupling material via

$$E_{\mathrm{THz}} \propto \theta_{\mathrm{SCC}} \left(j_s \times \frac{\mathbf{M}}{|\mathbf{M}|} \right) \tag{5}$$

where j_s is the spin current, **M** is the magnetization vector and θ_{SCC} is the spin-Hall angle for structures where the spin-Hall effect occurs,[14,66] such as in heavy metals. The latter is replaced by the inverse Rashba-Edelstein length (λ_{IREE}) for SCC by the inverse Rashba-Edelstein effect (IREE) in, for example, the surface states of TIs.[16,17,19,67,68]

Note that coherent THz emission spectroscopy measures directly the amplitude and phase of the generated pulses (unlike SHG) and has become a powerful non-contact technique to probe the current and spin-injection properties in complex spintronic heterostructures,[66] including 2D structures[69] to the examples above. In the studied heterostructures, the THz spintronic emision occurs owing to SCC at the TI interface and the TMD layer, and the THz nonlinear emission is a result of both the Bi_2Se_3 and WSe_2 layers. The THz emission of our samples was measured on ytterbium based OPA system (780 nm) with ZnTe electro-optic detection. An electromagnet was used to align domains in ferromagnetic layer (see Supporting Information for more information). All measurements were performed at room temperature.

We first present in **Figure 3**a the THz electric field emission from Bi_2Se_3/Co and Bi_2Se_3/WSe_2/Co compared to an optimised metallic spintronic structure of W/CoFeB/Pt (2/1.8/2 nm thick) to highlight the behaviour of nonlinear and magnetic response. Two set of curves for each sample is shown, corresponding to flipping of the applied magnetic field direction. For the metallic structure a change in sign of the THz phase is seen between opposite

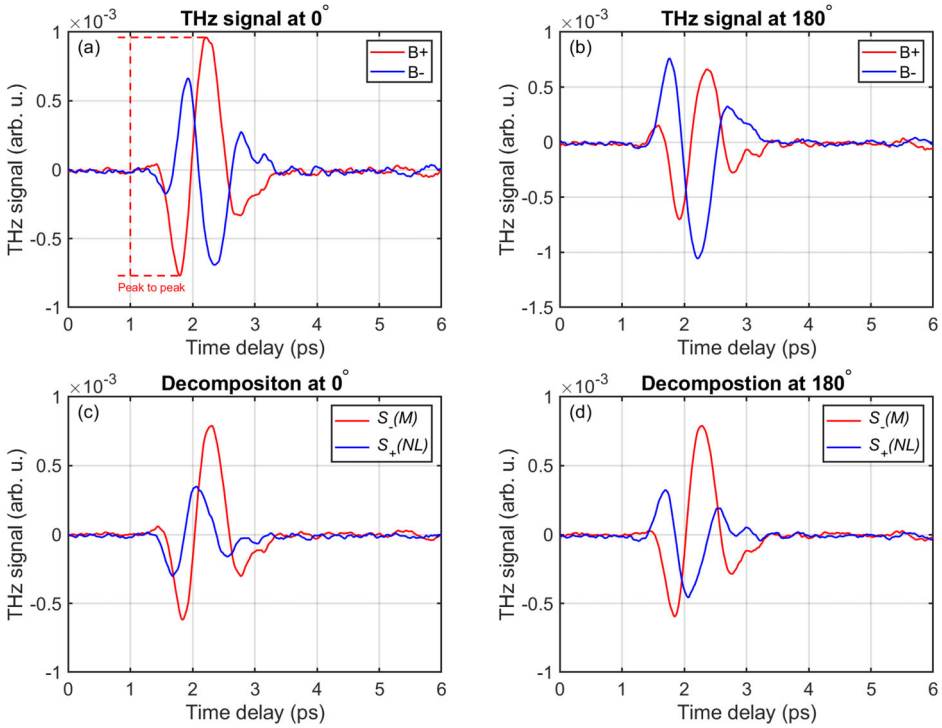

Figure 4. Example of extraction of magnetic $S_{-}(M)$ and nonlinear $S_{+}(NL)$ a,b) THz signal for sample Bi_2Se_3/WSe_2(2ML)/Co sample at two azimuth angles (0° and 180°). c,d) Extracted and decomposed into $S_{-}(M)$ and $S_{+}(NL)$ signals at the two angles using Equation (6).

magnetic directions, indicating a spin-charge conversion process and is entirely of magnetic origin. Compared to W/CoFeB/Pt, the THz phase obtained from Bi_2Se_3/Co is *i*) the same for a given magnetic field polarity, demonstrating an interconversion sign identical to the spin Hall effect sign of Pt, and *ii*) does not fully reverse with the magnetic field, i.e. the absolute value of the E-field amplitudes are not identical, which indicates the influence of the additional nonlinear optical contributions to the measured THz signal. The THz emitted signal from Bi_2Se_3/WSe_2(3ML)/Co shows the opposite extreme where no sign change in phase is observed and the signals for opposite applied magnetic fields are almost equal, indicating a small magnetic and large nonlinear component. The typical spectra for vdW structures are shown in the Figure 3(b), showing a bandwidth of ~ 3 THz limited by the optical excitation and detector. As discussed below, the nonlinear behaviour is enhanced in the heterostructures with WSe_2.

The nonlinear $S_{+}(NL)$ and magnetic $S_{-}(M)$ contributions to the time domain signal can be extracted[19] through the sum and difference, respectively, of the measured phase resolved THz signals at +B and -B applied magnetic field. (By changing the polarity of the magnetic field, the magnetization of Co follows the applied field direction owing to its soft magnetic character) i.e.:

$$S_{+}(NL) = \frac{S_{\mathrm{THz}}(+B) + S_{\mathrm{THz}}(-B)}{2} \quad \text{and}$$

$$S_{-}(M) = \frac{S_{\mathrm{THz}}(+B) - S_{\mathrm{THz}}(-B)}{2} \tag{6}$$

An example of the typical extraction of the nonlinear and magnetic components is shown in **Figure 4** for Bi_2Se_3/WSe_2(2ML)/Co sample. Figure 4a,b shows the acquired time domain signal for two different azimuthal angles, and Figure 4c,d shows the extracted magnetic contribution and the nonlinear contribution for each angle. Note the difference in phase of nonlinear emission between these particular azimuthal angles, whilst the THz emission of magnetic origin remains almost identical. From this extraction, Figure 3c shows peak-to-peak nonlinear and magnetic contributions as a function of the WSe_2 inset thickness, ranging from 0 to 4 ML, for their maximum measured values with sample azimuthal rotation (see below). The figure shows that the magnetic component $S_{-}(M)$ drops rapidly with WSe_2 layers as it acts as a spin barrier, while the nonlinear component $S_{+}(NL)$ increases with number of layers as each layer contributes to the nonlinear signal. Regarding the nonlinear component, the contribution of the TI itself is small, and a result of the second order nonlinearity of the TI surface states.[70,71] The nonlinear signal becomes dominated by the WSe_2 as a result of the enhanced second order nonlinearity of the interband excitations as highlighted by SHG investigations (e.g.),[24,25] and the calculated nonlinearity (see Supporting Information). Photon drag or surface field effects should not be observable owing to excitation at normal incidence, that is also highlighted through the measured and calculated azimuthal dependence (see below).

Beyond absolute values of the THz field, the effect of the WSe_2 polymorph on the emission symmetries of both magnetic $S_{-}(M)$ and nonlinear $S_{+}(NL)$ components were investigated by measuring the THz peak-to-peak field as a function of the crystallographic azimuthal angle ϕ. (Rotating the polarization of the pump beam also can show nonlinear processes and

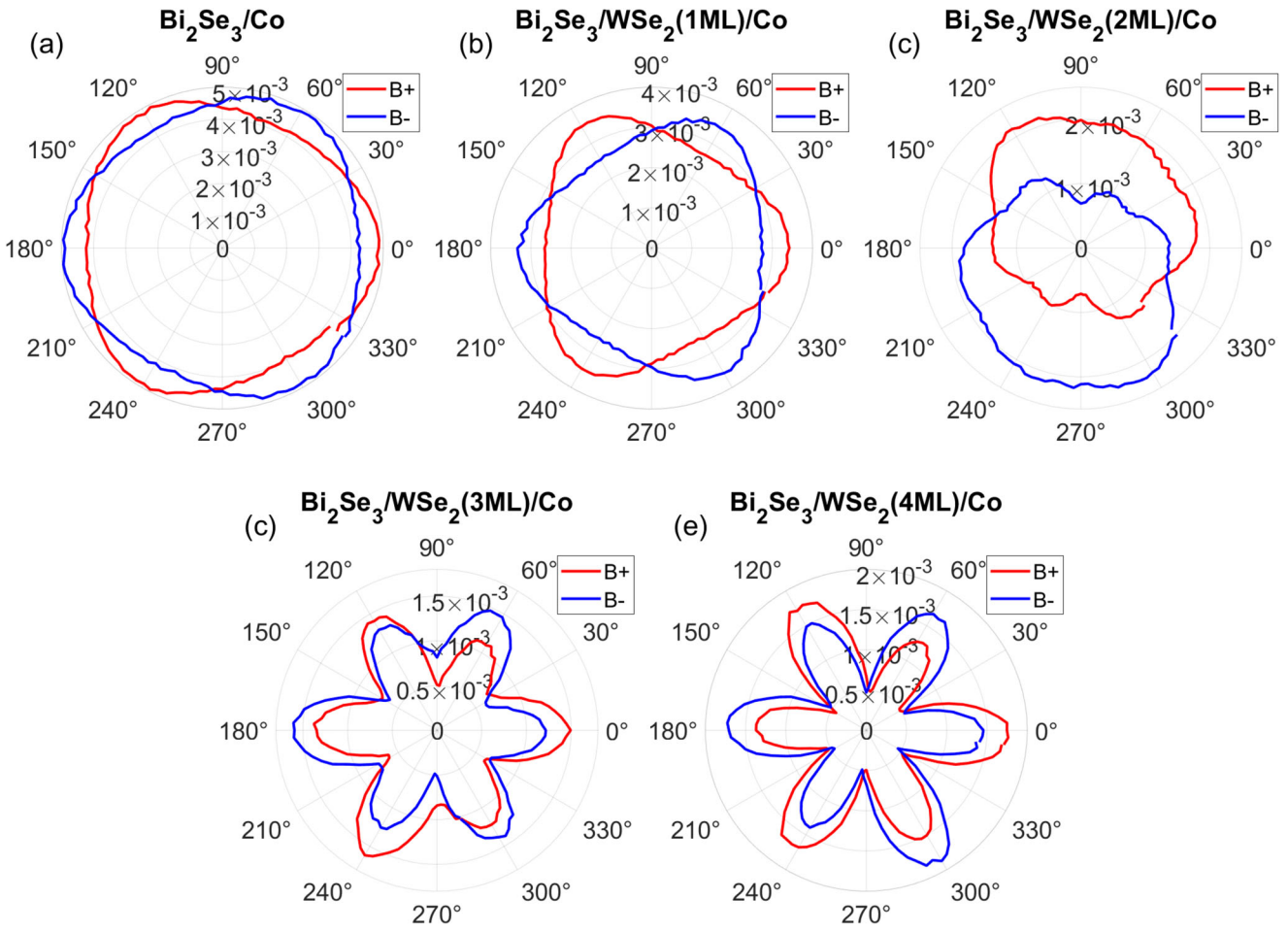

Figure 5. Peak-to-peak total amplitude in absolute values of emitted THz pulses from $Bi_2Se_3/WSe_2/Co$ heterostructures for thicknesses of WSe_2 ranging from 0 to 4 MLs (a-e) as a function of azimuthal angle rotation for two opposite orientations of the external magnetic field B±. The azimuth angle of the samples is oriented arbitrary, with positive lobe as origin.

symmetries).[38,72] The results are reported in **Figure 5** showing the peak-to-peak THz field values for two opposite magnetic field directions. Large changes are seen in the symmetries when transitioning from 0 ML to 4 MLs of inserted WSe_2. To decouple the magnetic and nonlinear components of the signals, we followed the same procedure as above (Figure 4 and Equation (6)) to compare the THz signals with opposite applied magnetic fields with the results shown below.

First, on the nonlinear contributions $S_+(NL)$ (**Figure 6**), we observe that on Bi_2Se_3/Co without the WSe_2 layer, the symmetries of the nonlinear contributions $S_+(NL)$ are sixfold with a small asymmetry between adjacent lobes, in agreement with previous studies of SHG from Bi_2Se_3 whose origin is from the surface states.[70] The red and blue points correspond to positive and negative values of the THz field respectively (see Supporting Information). The magnetic component is isotropic with rotation, as expected for spintronic emission (see Figure 8a). When a WSe_2 monolayer spacer is inserted in Figure 6, the nonlinear contribution is changed considerably owing to the WSe_2 high second-order electric susceptibility $\chi^{(2)} \simeq 5$ nm.V^{-1} determined through SHG[23] For increasing t_{TMD} we observe that the nonlinear contributions increases compared to Bi_2Se_3/Co, presenting a six-fold symmetry for 1, 3, and 4 ML. This corresponds to the expected three-fold symmetry for 2H and 3R polymorphs of WSe_2, as observed for SHG, noting that up to 2 MLs, WSe_2 shows a 2H form and increasing thicknesses show a mix of 2H and 3R polymorphs. As discussed above, space-inversion symmetry as a function of the parity of the WSe_2 ML thickness plays an important role. Indeed, for the 2H polymorph, an even number of MLs presents space-inversion symmetry (point group D_{3d}) and an odd number of MLs, WSe_2 breaks space-inversion symmetry (point group D_{3h}), whilst for the 3R case, space-inversion symmetry is always broken, as reported previously in refs. [23,73]. Therefore, a six fold optical emission response based on optical nonlinearities is expected for any 3R form and only for odd number of layers for the 2H polymorph. However, for WSe_2(2ML), not only a strong second order response is observed but the symmetry drastically changes to twofold, which would be incompatible with nonlinearities for 2H geometries and for an even number of WSe_2 layers. This second order effect is therefore solely owing to the 1T′ polymorph observed in these layers that is expected to give a twofold symmetry (see Table 1). In 1T′ form, the trend of layer dependent SHG is opposite to that in 2H phase i.e., even layers of 1T′ with inversion symmetry breaking display

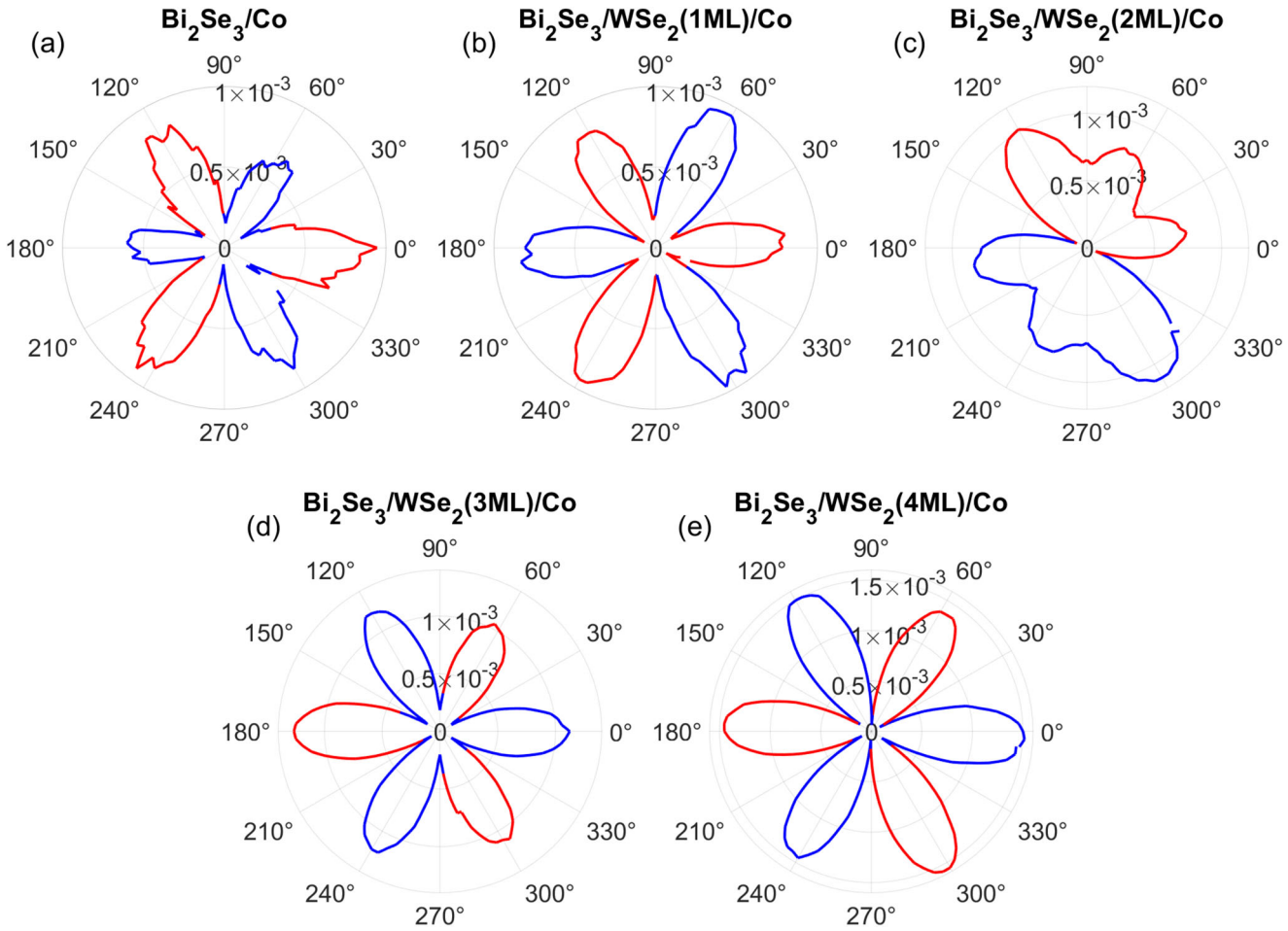

Figure 6. Peak to peak amplitudes of the nonlinear components of the THz signal $S_+(NL)$ decomposed by Equation (6)), for samples with different number of WSe_2 layers, a–e) corresponding to 0 – 4 ML. The color of lines represents positive (red) and negative (blue) polarity (see Supporting Information).

significant SHG while odd layers with inversion symmetry show negligible SHG.[23,74] Note that 4 MLs WSe_2 sample shows a three fold symmetry as the 3R polymorph is dominant and where the 2H polymorph is expected to give a zero nonlinearity owing to the symmetry. Therefore, this works shows how the THz nonlinearities in these junctions can be controlled at the monolayer level through the structural polymorphs of WSe_2 and stacking order. We emphasize that the thickness-dependent THz emission (down-conversion) is reported here for the first time where all previous works have been on SHG, showing the high crystalline quality of the material, highlighted by the fact that the nonlinearities are present over large areas (THz spot size ≈ 1000 µm). This shows also that THz emission spectroscopy and its inherent polarization sensitivity can be an powerful probe to determine the thickness parity and symmetries of 2D materials on macroscopic scales.

The 2 ML nonlinear form can be further analysed to extract the exact contribution of the WSe_2 layers by removing the contribution from the TI. **Figure** 7a shows the THz emission of the 2 ML sample on a cartesian plot. Here, removing from the raw data the nonlinear contribution from the Bi_2Se_3 layers as cos (3ϕ) (grey dashed curve), results in the nonlinear contribution of WSe_2 (orange curve). The data is plotted in polar coordinates in Figure 7b, that shows a clear twofold geometry as expected for a 1T′ polymorph of WSe_2 (see Table 1) and can be fitted with Equation (2). Note that although 1T′ WSe_2 likely grows in three domains, oriented every 120° on Bi_2Se_3, the observed twofold symmetry demonstrates that one domain orientation dominates. This preferential domain orientation is due to the vicinal character of the sapphire surface that appears to favor one domain orientation.[36] Indeed the miscut axis has been found along ϕ ≈ 150° by x-ray diffraction which is orthogonal to the anisotropy axis experimentally observed in the nonlinear THz component of Figure 6c.

Regarding the magnetic contribution of the THz signal (**Figure** 8), this can be correlated to the efficiency of the spin injection and spin-charge conversion processes. First, the decrease of the magnetic contribution with WSe_2 thickness is a result of the formation of an energy barrier,[69] which prevents an efficient spin-injection from Co to Bi_2Se_3 where interfacial conversion occur. For 4 MLs WSe_2, the signal from the magnetic component stops decreasing, suggesting that the emission comes from the self emission of the ferromagnetic layer[75] and that no spin current is injected through WSe_2 layers. (Although the magnetic

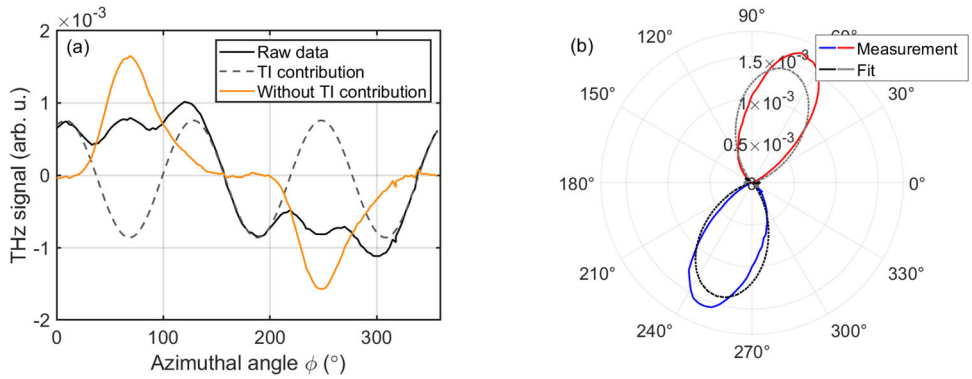

Figure 7. Nonlinear Contribution of 1T′ WSe_2 a) THz amplitude as a function of azimuthal angle ϕ for the Bi_2Se_3/WSe_2(2ML)/Co heterostructure showing the acquired nonlinear behaviour (black), the TI contribution (grey dash), and the extracted contribution for WSe_2 only (orange). b) Polar plot of WSe_2 emission showing only a two lobe patten as expected for the 1T′ polymorph - Table 1. The dotted line is a fit to the data from Equation (2) with grey (black) corresponding to positive (negative) values.

contributions reduce as WSe_2 acts as a barrier, this can be overcome through the growth of 2D ferromagnets on top of the TI, followed by the TMD growth such that both the TMD and TI emission can contribute additionally). Second, Figure 8 also shows that the magnetic contribution is not entirely isotropic for 1 and 2 ML of WSe_2, which is not the case of the sample without WSe_2 layers or for the 3 ML and 4 ML WSe_2 samples (see Supporting Information), and suggests another magnetic phenomena in the measured THz field. This is highlighted by subtracting the mean value of the THz field from the magnetic contribution, as shown in Figure 8, with the colors showing positive (red) and negative (blue) values. As can be observed in the 1 ML and 2 ML WSe_2 structures, the symmetry appears to resemble the form observed for the 2 ML nonlinear contribution but with opposite phase and without a contribution of Bi_2Se_3 (Figure 7). This suggests that the form is related to the 1T′ phase of WSe_2 and its high anisotropic nature but of magnetic origin. Indeed the curves can be fitted with Equation (2) that corresponds to the 1T′ polymorph. The treatment of the data through Equation (6) of the magnetic component removes the intrinsic part of the nonlinearity. With the constant part removed, this leaves only the magnetic nonlinearity $\chi_c^{(2)}$. As the form is exactly the same as the intrinsic nonlinearity $\chi_i^{(2)}$ and that WSe_2 is not itself magnetic, this suggests that the magnetic properties are induced by the proximity of the TMD with the FM most likely as a result of spin-dependent exchange coupling between the two layers, leading to a net magnetic moment on the TMD.[22,76] Further, the opposite phase of the magnetic component suggests that a positive magnetic field gives a slightly smaller nonlinearity than negative fields i.e. $\chi_c^{(2)}$(+B) is negative and $\chi_c^{(2)}$(-B) is positive. The measured difference in magnetic and non magnetic nonlinearity is approximately an order of magnitude giving therefore a magnetic nonlinearity ten times smaller. Interestingly the sixfold symmetry from the 2H or 3R polymorph are not observed, highlighting that the nonlinearity of this polymorph is considerably smaller. This highlights the application of THz phase-resolved measurements to probe subtle magnetic nonlinear effects and the relevance of the polymorph on the magnetic nonlinearity. Although relatively small in this first THz demonstration, recent proposals highlight that magnetic nonlinearities can become comparable to electronic ones

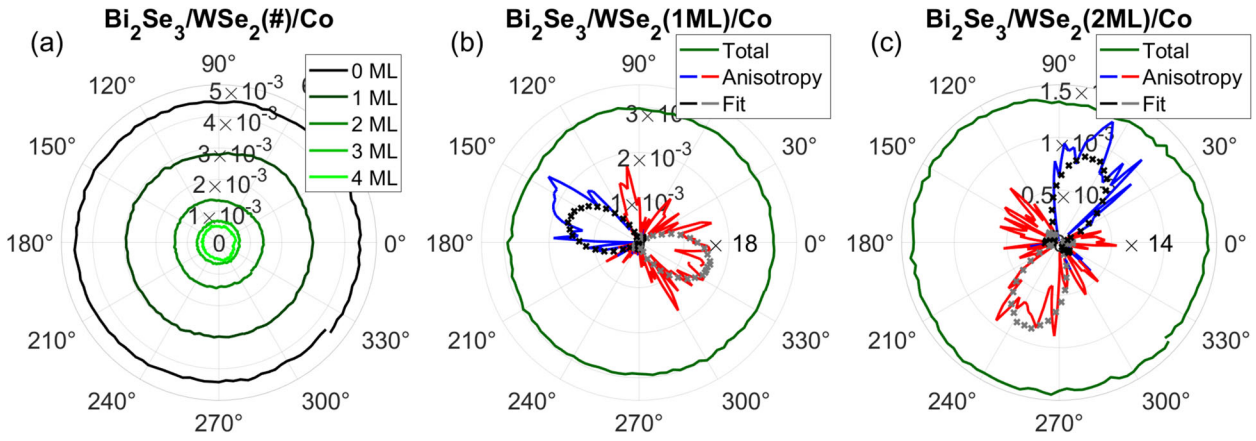

Figure 8. Peak to peak amplitudes of the magnetic components of the THz signal $S_-(M)$ decomposed by Equation (6)) for a) all samples with different number of WSe_2 layers. b,c) Comparison of anisotropic component of magnetic signal for 1 and 2 ML obtained by removing the isotropic part (i.e., average value of green curve). The dotted line is a fit to the data from Equation (2) with grey (black) corresponding to positive (negative) values).

in 2D materials with the role of stacking order, polymorph, and spin-orbit coupling being important.[77]

Note that the observed behavior could be considered as an extra spin-to-charge conversion process in the anisotropic 1T′ polymorph of WSe_2. Indeed, a considerable body of work has shown that with materials of reduced symmetry such as the 1T′ investigated here demonstrate an anisotropic response in their spintronic properties (as well as optical, electrical, magnetic etc).[78] This has been concentrated on spin-to-charge conversion in the Te family (e.g., WTe_2 and $MoTe_2$) that has a distorted crystal structure as in 1T′ WSe_2. For example, junctions of WTe_2/FM have shown that charge conductivity, spin conductivity, and spin-to-charge conversion is anisotropic and differs from the isotropic states of topological insulators.[79–82] However, owing to the symmetry of the structure, a rotation of 180° of the sample would lead to exactly the same sign of the generated current. Therefore, a $cos^2(\phi)$ type dependence would be expected if there was an anisotropic spin-to-charge conversion contribution, rather than the $cos(\phi)$ observed here. Although there could be other spin-to-charge phenomena, in this current work, these appear quite weak, possibly owing to the WSe_2 acting as a spin barrier. Nonetheless, the 1T′ anisotropy clearly leads to magnetic dependent nonlinearity as a result of proximity effects with the FM.

Conclusion

We have demonstrated the realization of complex heterostructures of vdW materials and their polymorphs, showing high-quality large-area growth, where multiple physical phenomena can be combined over macroscopic surface areas. This is demonstrated in their giant nonlinearities, THz spintronics in topological insulators, and magnetic proximity effects in reduced symmetry materials. Each of these magnetic and nonlinear contributions could be extracted using the THz phase resolved emission nature of the experiment, highlighting multiple THz generation phenomena within a heterostructure stack. The current work demonstrates the principle of this scalable approach of combining different materials through growth techniques. In principle, there is no limitation to grow any TMD/TI bilayer system since, in the van der Waals epitaxy regime, lattice matching requirement between epilayers is alleviated, although growth order may vary. A wide range of perspectives from this base of vdW heterotructure engineering will be possible with the first steps in more complex heterostructures with, for example, multiple periods to enhance the effects and combination with 2D ferromagnetics.[83,84] Longterm this work can be combined with other phenomena, such as the coupling with ferroelectricity, phononics and coherent current control to the effects already observed, which could be further manipulated either by a gate or through the excitation wavelength. Further, spatially resolved nanoscale terahertz emission spectroscopy[85] would be of interest to show the role of single crystal domains and its relevance to macroscopic effects, as well as highlighting further the uniformity of the samples. This work opens up important prospects of new types of interfaces and devices on technological relevant levels, where the entire properties of the material can be artificially designed and controlled.

Supporting Information

Supporting Information is available from the Wiley Online Library or from the author.

Acknowledgements

M.M. and A.W. contributed equally to this work. The authors acknowledged funding from European Union's Horizon 2020 research and innovation program under grant agreement No. 964735 (FET-OPEN EXTREME-IR) and the French National Research Agency (ANR) under ANR-22-CE30-0026 DYNTOP and ANR-21-CE24-011 TRAPIST. This work was supported by a government grant managed by the ANR as part of the France 2030 investment plan from PEPR SPIN ANR-22-EXSP-0002. This work was granted access to the HPC resources of MesoPSL financed by the Region Ile de France and the project EquipMeso (reference ANR-10-EQPX-29-01) of the programme Investissements d'Avenir supervised by the Agence Nationale pour la Recherche. The authors acknowledged funding from the European Union's Horizon 2020 research and innovation program under grant agreement No. 881603 (Graphene Flagship) and No. 101099552 (HORIZON-EIC-2022-PATHFINDEROPEN-01-01 PLASNANO). The French National Research Agency (ANR) was acknowledged for its support through the ESR/EQUIPEX+ ANR-21-ESRE-0025 2D-MAG project. The LANEF framework (No. ANR-10-LABX-0051) was acknowledged for its support with mutualized infrastructure.

Conflict of Interest

The authors declare no conflict of interest.

Data Availability Statement

The data that support the findings of this study are available from the corresponding author upon reasonable request.

Keywords

giant nonlinearities, material Polymorphs, phase engineering, spintronics, terahertz

Received: March 30, 2025
Revised: August 25, 2025
Published online: September 19, 2025

[1] A. K. Geim, I. V. Grigorieva, *Nature* **2013**, *499*, 419.
[2] K. S. Novoselov, A. Mishchenko, A. Carvalho, A. H. C. Neto, *Science* **2016**, *353*, aac9439.
[3] A. Castellanos-Gomez, X. Duan, Z. Fei, H. R. Gutierrez, Y. Huang, X. Huang, J. Quereda, Q. Qian, E. Sutter, P. Sutter, *Nat. Rev. Methods Primers* **2022**, *2*, 58.
[4] H.-L. Hou, C. Anichini, P. Samorí, A. Criado, M. Prato, *Adv. Funct. Mater.* **2022**, *32*, 2207065.
[5] P. Wang, C. Jia, Y. Huang, X. Duan, *Matter* **2021**, *4*, 552.
[6] Z. C. Wenzhuo Zhuang, X. Wang, *Adv. Phys.: X* **2022**, *7*, 2034529.
[7] J. Li, X. Yang, Z. Zhang, W. Yang, X. Duan, X. Duan, *Nat. Mater.* **2024**, *23*, 1326.
[8] G. Xue, B. Qin, C. Ma, P. Yin, C. Liu, K. Liu, *Chem. Rev.* **2024**, *124*, 9785.
[9] J. E. Moore, *Nature* **2010**, *464*, 194.

[10] S. Manzeli, D. Ovchinnikov, D. Pasquier, O. V. Yazyev, A. Kis, *Nat. Rev. Mater.* **2017**, *2*, 17033.
[11] G. Bihlmayer, P. Noël, D. V. Vyalikh, E. V. Chulkov, A. Manchon, *Nat. Rev. Phys.* **2022**, *4*, 642.
[12] M. Z. Hasan, C. L. Kane, *Rev. Mod. Phys.* **2010**, *82*, 3045.
[13] Q. Zhang, Z. Zhang, Z. Zhu, U. Schwingenschlögl, Y. Cui, *ACS Nano* **2012**, *6*, 2345.
[14] T. Seifert, S. Jaiswal, U. Martens, J. Hannegan, L. Braun, P. Maldonado, F. Freimuth, A. Kronenberg, J. Henrizi, I. Radu, E. Beaurepaire, Y. Mokrousov, P. M. Oppeneer, M. Jourdan, G. Jakob, D. Turchinovich, L. M. Hayden, M. Wolf, M. Münzenberg, M. Kläui, T. Kampfrath, *Nat. Photonics* **2016**, *10*, 483.
[15] T. G. Park, J. H. Jeon, S.-H. Chun, S. Lee, F. Rotermund, *Commun. Phys.* **2022**, *5*, 182.
[16] X. Wang, L. Cheng, D. Zhu, Y. Wu, M. Chen, Y. Wang, D. Zhao, C. B. Boothroyd, Y. M. Lam, J.-X. Zhu, M. Battiato, J. C. W. Song, H. Yang, E. E. M. Chia, *Adv. Mater.* **2018**, *30*, 1802356.
[17] M. Tong, Y. Hu, Z. Wang, T. Zhou, X. Xie, X. Cheng, T. Jiang, *Nano Lett.* **2020**, *20*, 8503.
[18] E. Rongione, L. Baringthon, D. She, G. Patriarche, R. Lebrun, A. Lemaître, M. Morassi, N. Reyren, M. mičica, J. Mangeney, J. Tignon, F. Bertran, S. Dhillon, P. Le Févre, H. Jaffrés, J.-M. George, *Adv. Sci.* **2023**, *10*, 2301124.
[19] E. Rongione, S. Fragkos, L. Baringthon, J. Hawecker, E. Xenogiannopoulou, P. Tsipas, C. Song, M. Mičica, J. Mangeney, J. Tignon, T. Boulier, N. Reyren, R. Lebrun, J. George, P. Le Févre, S. Dhillon, A. Dimoulas, H. Jaffrés, *Adv. Opt. Mater.* **2022**, *10*, 2102061.
[20] K. Abdukayumov, M. Mičica, F. Ibrahim, L. Vojáček, C. Vergnaud, A. Marty, J.-Y. Veuillen, P. Mallet, I. G. de Moraes, D. Dosenovic, S. Gambarelli, V. Maurel, A. Wright, J. Tignon, J. Mangeney, A. Ouerghi, V. Renard, F. Mesple, J. Li, F. Bonell, H. Okuno, M. Chshiev, J.-M. George, H. Jaffrés, S. Dhillon, M. Jamet, *Adv. Mater.* **2024**, *n/a*, 2304243.
[21] B. Huang, M. A. McGuire, A. F. May, D. Xiao, P. Jarillo-Herrero, X. Xu, *Nat. Mater.* **2020**, *19*, 1276.
[22] C. Lee, F. Katmis, P. Jarillo-Herrero, J. S. Moodera, N. Gedik, *Nat. Commun.* **2016**, *7*, 12014.
[23] J. Ribeiro-Soares, C. Janisch, Z. Liu, A. L. Elías, M. S. Dresselhaus, M. Terrones, L. G. Cançado, A. Jorio, *2D Mater.* **2015**, *2*, 045015.
[24] G. Wang, X. Marie, I. Gerber, T. Amand, D. Lagarde, L. Bouet, M. Vidal, A. Balocchi, B. Urbaszek, *Phys. Rev. Lett.* **2015**, *114*, 097403.
[25] J. K. Day, M.-H. Chung, Y.-H. Lee, V. M. Menon, *Opt. Mater. Express* **2016**, *6*, 2360.
[26] H. Chen, V. Corboliou, A. S. Solntsev, D.-Y. Choi, M. A. Vincenti, D. de Ceglia, C. de Angelis, Y. Lu, D. N. Neshev, *Light: Sci. Appl.* **2017**, *6*, e17060.
[27] M. C. Lucking, K. Beach, H. Terrones, *Sci. Rep.* **2018**, *8*, 10118.
[28] J. Shi, Y.-Q. Bie, A. Zong, S. Fang, W. Chen, J. Han, Z. Cao, Y. Zhang, T. Taniguchi, K. Watanabe, X. Fu, V. Bulović, E. Kaxiras, E. Baldini, P. Jarillo-Herrero, K. A. Nelson, *Nat. Commun.* **2023**, *14*, 5905.
[29] Y. A. Eshete, K. Kang, S. Kang, Y. Kim, P. L. Nguyen, D.-Y. Cho, Y. Kim, J. Lee, S. Cho, H. Yang, *Adv. Mater.* **2022**, *34*, 2202633.
[30] B. Küçüköz, B. Munkhbat, T. O. Shegai, *ACS Photonics* **2022**, *9*, 518.
[31] D. E. Wilcox, M. E. Sykes, A. Niedringhaus, M. Shtein, J. P. Ogilvie, *Opt. Lett.* **2014**, *39*, 4274.
[32] R. Mankowsky, A. von Hoegen, M. Först, A. Cavalleri, *Phys. Rev. Lett.* **2017**, *118*, 197601.
[33] F. Liu, W. Wu, Y. Bai, S. H. Chae, Q. Li, J. Wang, J. Hone, X.-Y. Zhu, *Science* **2020**, *367*, 903.
[34] F. Liu, *Prog. Surf. Sci.* **2021**, *96*, 100626.
[35] T. Handa, C.-Y. Huang, Y. Li, N. Olsen, D. G. Chica, D. D. Xu, F. Sturm, J. W. McIver, X. Roy, X. Zhu, *Nat. Mater.* **2025**, *24*, 1203.
[36] B. Qin, C. Ma, Q. Guo, X. Li, W. Wei, C. Ma, Q. Wang, F. Liu, M. Zhao, G. Xue, J. Qi, M. Wu, H. Hong, L. Du, Q. Zhao, P. Gao, X. Wang, E. Wang, G. Zhang, C. Liu, K. Liu, *Science* **2024**, *385*, 99.
[37] M. Hemmat, S. Ayari, M. Mičica, H. Vergnet, S. Guo, M. Arfaoui, X. Yu, D. Vala, A. Wright, K. Postava, J. Mangeney, F. Carosella, S. Jaziri, Q. J. Wang, Z. Liu, J. Tignon, R. Ferreira, E. Baudin, S. Dhillon, *InfoMat* **2023**, *5*, e12468.
[38] Y. Huang, L. Zhu, Q. Zhao, Y. Guo, Z. Ren, J. Bai, X. Xu, *ACS Appl. Mater. Interfaces* **2017**, *9*, 4956.
[39] J. Pettine, P. Padmanabhan, N. Sirica, R. P. Prasankumar, A. J. Taylor, H.-T. Chen, *Light: Sci. Appl.* **2023**, *12*, 133.
[40] J. Yang, S. Jiang, J. Xie, H. Jiang, S. Xu, K. Zhang, Y. Shi, Y. Zhang, Z. Zeng, G. Fang, T. Wang, F. Su, *ACS Nano* **2021**, *15*, 16760.
[41] C. J. Docherty, P. Parkinson, H. J. Joyce, M.-H. Chiu, C.-H. Chen, M.-Y. Lee, L.-J. Li, L. M. Herz, M. B. Johnston, *ACS Nano* **2014**, *8*, 11147.
[42] X. Yu, P. Yu, D. Wu, B. Singh, Q. Zeng, H. Lin, W. Zhou, J. Lin, K. Suenaga, Z. Liu, Q. J. Wang, *Nat. Commun.* **2018**, *9*, 1545.
[43] S. Zhu, R. Duan, W. Chen, F. Wang, J. Han, X. Xu, L. Wu, M. Ye, F. Sun, S. Han, X. Zhao, C. S. Tan, H. Liang, Z. Liu, Q. J. Wang, *ACS Nano* **2023**, *17*, 2148.
[44] N. Yoshikawa, K. Nagai, K. Uchida, Y. Takaguchi, S. Sasaki, Y. Miyata, K. Tanaka, *Nat. Commun.* **2019**, *10*, 3709.
[45] R. Yue, Y. Nie, L. A. Walsh, R. Addou, C. Liang, N. Lu, A. T. Barton, H. Zhu, Z. Che, D. Barrera, L. Cheng, P.-R. Cha, Y. J. Chabal, J. W. P. Hsu, J. Kim, M. J. Kim, L. Colombo, R. M. Wallace, K. Cho, C. L. Hinkle, *2D Mater.* **2017**, *4*, 045019.
[46] R. Galceran, F. Bonell, L. Camosi, G. Sauthier, Z. M. Gebeyehu, M. J. Esplandiu, A. Arrighi, I. Fernández Aguirre, A. I. Figueroa, J. F. Sierra, S. O. Valenzuela, *Adv. Mater. Interfaces* **2022**, *9*, 2201997.
[47] R. Sun, S. Yang, X. Yang, E. Vetter, D. Sun, N. Li, L. Su, Y. Li, Y. Li, Z.-z. Gong, Z.-k. Xie, K.-y. Hou, Q. Gul, W. He, X.-q. Zhang, Z.-h. Cheng, *Nano Lett.* **2019**, *19*, 4420.
[48] J. Hawecker, T.-H. Dang, E. Rongione, J. Boust, S. Collin, J.-M. George, H.-J. Drouhin, Y. Laplace, R. Grasset, J. Dong, J. Mangeney, J. Tignon, H. Jaffrés, L. Perfetti, S. Dhillon, *Adv. Opt. Mater.* **2021**, *9*, 2100412.
[49] J. H. Kim, H. Sung, G.-H. Lee, *Small Sci.* **2024**, *4*, 2300093.
[50] J. Lim, J.-I. Lee, Y. Wang, N. Gauriot, E. Sebastian, M. Chhowalla, C. Schnedermann, A. Rao, *Nature* **2024**, *633*, 83.
[51] J. Zhang, L. Wang, J. Lü, Z. Wang, H. Wu, G. Zhu, N. Wang, F. Xue, X. Zeng, L. Zhu, Y. Hu, X. Deng, C. Guan, C. Yang, Z. Lin, P. Wang, B. Zhou, J. Lü, W. Zhu, X. Zhang, Y. Huang, W. Huang, Y. Peng, X. Duan, *Nat. Mater.* **2025**, *24*, 369.
[52] Z. Sun, C. Hong, Y. Chen, Z. Sheng, S. Wu, Z. Wang, B. Liang, W.-T. Liu, Z. Yuan, Y. Wu, Q. Mi, Z. Liu, J. Shen, S. Wu, *Nat. Mater.* **2025**, *24*, 226.
[53] Z. Zeng, X. Sun, D. Zhang, W. Zheng, X. Fan, M. He, T. Xu, L. Sun, X. Wang, A. Pan, *Adv. Funct. Mater.* **2019**, *29*, 1806874.
[54] R. Beams, L. G. Cançado, S. Krylyuk, I. Kalish, B. Kalanyan, A. K. Singh, K. Choudhary, A. Bruma, P. M. Vora, F. Tavazza, A. V. Davydov, S. J. Stranick, *ACS Nano* **2016**, *10*, 9626.
[55] D. Hou, Z. Jiang, R. Xiao, C. Liu, X. Chang, Y. Liu, Z. Wang, B. Li, X. Liu, X. Hu, W. Ding, J. Hu, X. Luo, Y. Sun, Z. Sheng, *Adv. Opt. Mater.* **2024**, *12*, 2400943.
[56] S. Toyoda, M. Fiebig, T. hisa Arima, Y. Tokura, N. Ogawa, *Sci. Adv.* **2021**, *7*, eabe2793.
[57] P.-C. Yeh, W. Jin, N. Zaki, D. Zhang, J. T. Liou, J. T. Sadowski, A. Al-Mahboob, J. I. Dadap, I. P. Herman, P. Sutter, R. M. Osgood, *Phys. Rev. B* **2015**, *91*, 041407.
[58] A. Ramasubramaniam, *Phys. Rev. B* **2012**, *86*, 115409.
[59] J. He, K. Hummer, C. Franchini, *Phys. Rev. B* **2014**, *89*, 075409.
[60] P. Chen, W. W. Pai, Y.-H. Chan, W.-L. Sun, C.-Z. Xu, D.-S. Lin, M. Y. Chou, A.-V. Fedorov, T.-C. Chiang, *Nat. Commun.* **2018**, *9*, 2003.

[61] M. M. Ugeda, A. Pulkin, S. Tang, H. Ryu, Q. Wu, Y. Zhang, D. Wong, Z. Pedramrazi, A. Martín-Recio, Y. Chen, F. Wang, Z.-X. Shen, S.-K. Mo, O. V. Yazyev, M. F. Crommie, *Nat. Commun.* **2018**, *9*, 3401.
[62] Y. Wan, J.-H. Fu, C.-P. Chuu, V. Tung, Y. Shi, L.-J. Li, *Chem. Soc. Rev.* **2022**, *51*, 803.
[63] S. Tang, C. Zhang, D. Wong, Z. Pedramrazi, H.-Z. Tsai, C. Jia, B. Moritz, M. Claassen, H. Ryu, S. Kahn, J. Jiang, H. Yan, M. Hashimoto, D. Lu, R. G. Moore, C.-C. Hwang, C. Hwang, Z. Hussain, Y. Chen, M. M. Ugeda, Z. Liu, X. Xie, T. P. Devereaux, M. F. Crommie, S.-K. Mo, Z.-X. Shen, *Nat. Phys.* **2017**, *13*, 683.
[64] W. Chen, X. Xie, J. Zong, T. Chen, D. Lin, F. Yu, S. Jin, L. Zhou, J. Zou, J. Sun, X. Xi, Y. Zhang, *Sci. Rep.* **2019**, *9*, 2685.
[65] W. Zhao, Z. Ghorannevis, K. K. Amara, J. R. Pang, M. Toh, X. Zhang, C. Kloc, P. H. Tan, G. Eda, *Nanoscale* **2013**, *5*, 9677.
[66] T. H. Dang, J. Hawecker, E. Rongione, G. Baez Flores, D. Q. To, J. C. Rojas-Sanchez, H. Nong, J. Mangeney, J. Tignon, F. Godel, S. Collin, P. Seneor, M. Bibes, A. Fert, M. Anane, J.-M. George, L. Vila, M. Cosset-Cheneau, D. Dolfi, R. Lebrun, P. Bortolotti, K. Belashchenko, S. Dhillon, H. Jaffrés, *Appl. Phys. Rev.* **2020**, *7*, 041409.
[67] C. Zhou, Y. P. Liu, Z. Wang, S. J. Ma, M. W. Jia, R. Q. Wu, L. Zhou, W. Zhang, M. K. Liu, Y. Z. Wu, J. Qi, *Phys. Rev. Lett.* **2018**, *121*, 086801.
[68] X. Chen, H. Wang, C. Wang, C. Ouyang, G. Wei, T. Nie, W. Zhao, J. Miao, Y. Li, L. Wang, X. Wu, *Adv. Photonics Res.* **2021**, *2*, 2000099.
[69] L. Cheng, X. Wang, W. Yang, J. Chai, M. Yang, M. Chen, Y. Wu, X. Chen, D. Chi, K. E. J. Goh, J.-X. Zhu, H. Sun, S. Wang, J. C. W. Song, M. Battiato, H. Yang, E. E. M. Chia, *Nat. Phys.* **2019**, *15*, 347.
[70] D. Hsieh, J. W. McIver, D. H. Torchinsky, D. R. Gardner, Y. S. Lee, N. Gedik, *Phys. Rev. Lett.* **2011**, *106*, 057401.
[71] L. Braun, G. Mussler, A. Hruban, M. Konczykowski, T. Schumann, M. Wolf, M. Münzenberg, L. Perfetti, T. Kampfrath, *Nat. Commun.* **2016**, *7*, 13259.
[72] E. M. Mannebach, K.-A. N. Duerloo, L. A. Pellouchoud, M.-J. Sher, S. Nah, Y.-H. Kuo, Y. Yu, A. F. Marshall, L. Cao, E. J. Reed, A. M. Lindenberg, *ACS Nano* **2014**, *8*, 10734.
[73] H. G. Rosa, Y. W. Ho, I. Verzhbitskiy, M. J. F. L. Rodrigues, T. Taniguchi, K. Watanabe, G. Eda, V. M. Pereira, J. C. V. Gomes, *Sci. Rep.* **2018**, *8*, 10035.
[74] Y. Song, S. Hu, M.-L. Lin, X. Gan, P.-H. Tan, J. Zhao, *ACS Photonics* **2018**, *5*, 3485.
[75] W. Zhang, P. Maldonado, Z. Jin, T. S. Seifert, J. Arabski, G. Schmerber, E. Beaurepaire, M. Bonn, T. Kampfrath, P. M. Oppeneer, D. Turchinovich, *Nat. Commun.* **2020**, *11*, 4247.
[76] D. Zhong, K. L. Seyler, X. Linpeng, N. P. Wilson, T. Taniguchi, K. Watanabe, M. A. McGuire, K.-M. C. Fu, D. Xiao, W. Yao, X. Xu, *Nat. Nanotechnol.* **2020**, *15*, 187.
[77] D. Wu, M. Ye, H. Chen, Y. Xu, W. Duan, *npj Comput. Mater.* **2024**, *10*, 79.
[78] C. S. Tang, X. Yin, A. T. S. Wee, *Appl. Phys. Rev.* **2021**, *8*, 011313.
[79] P. Li, W. Wu, Y. Wen, C. Zhang, J. Zhang, S. Zhang, Z. Yu, S. A. Yang, A. Manchon, X.-x. Zhang, *Nat. Commun.* **2018**, *9*, 3990.
[80] D. MacNeill, G. M. Stiehl, M. H. D. Guimaraes, R. A. Buhrman, J. Park, D. C. Ralph, *Nat. Phys.* **2017**, *13*, 300.
[81] B. Zhao, D. Khokhriakov, Y. Zhang, H. Fu, B. Karpiak, A. M. Hoque, X. Xu, Y. Jiang, B. Yan, S. P. Dash, *Phys. Rev. Res.* **2020**, *2*, 013286.
[82] C. K. Safeer, N. Ontoso, J. Ingla-Aynés, F. Herling, V. T. Pham, A. Kurzmann, K. Ensslin, A. Chuvilin, I. Robredo, M. G. Vergniory, F. de Juan, L. E. Hueso, M. R. Calvo, F. Casanova, *Nano Lett.* **2019**, *19*, 8758.
[83] X. Chen, X. Zhang, G. Xiang, *Nanoscale* **2024**, *16*, 527.
[84] Q. Guillet, L. Vojáček, D. Dosenovic, F. Ibrahim, H. Boukari, J. Li, F. Choueikani, P. Ohresser, A. Ouerghi, F. Mesple, V. Renard, J.-F. m. c. Jacquot, D. Jalabert, H. Okuno, M. Chshiev, C. Vergnaud, F. Bonell, A. Marty, M. Jamet, *Phys. Rev. Mater.* **2023**, *7*, 054005.
[85] P. Klarskov, H. Kim, V. L. Colvin, D. M. Mittleman, *ACS Photonics* **2017**, *4*, 2676.